Oxidation Aspects of the Lime-Concentrate-Pellet Roasting Process

H. AHMADZAI, S. BLAIRS, B. HARRIS, and L-I STAFFANSSON

Thermogravimetry has been employed to follow the progress of the oxidation reaction of cylindrical pellets of chalcopyrite concentrate blended with lime. Metallographic examination of pellet sections established the shrinking core pattern under the various experimental conditions. The rate of oxidation was investigated over the temperature range 753 to 873 K. To enable comparison with earlier work, subsequent leaching of calcines from the 773 K runs was also examined. Factors resulting in low copper recoveries have been examined thermodynamically and confirmed by X-ray diffraction analyses.

I. INTRODUCTION

INCREASING anthropogenic emission of gaseous sulfur compounds into the environment has resulted in a spate of developments for handling the "sulfate" problem. To meet abatement standards in the extraction of copper, combined pyrometallurgical and hydrometallurgical processing have featured prominently.[1,2,3] One such development, the Lime-Concentrate-Pellet-Roast Process (L.C.P.R.-Process),[4–8] involves fixation of sulfur in copper sulfide concentrates at the source in an innocuous form using lime:

$$CuFeS_2 + \frac{17}{4}O_2 + \frac{3}{2}Ca(OH)_2 \rightarrow \frac{1}{2}CuO\cdot CuSO_4 + \frac{1}{2}Fe_2O_3 + \frac{3}{2}CaSO_4 + \frac{3}{2}H_2O \qquad [1]$$

Copper concentrates and lime in granulated and ungranulated form were first investigated by the Rumanians at temperatures in the range 973 to 1123 K.[9] Subsequent application of alkalies to the sulfatizing step of the Roast-Leach-Electrowinning (R.L.E) Process was proposed by the United States Bureau of Mines.[10] $Ca(OH)_2$ was found to be most effective in retaining up to 98 wt pct of the sulfur as anhydrite (Table I). Bartlett and Haung[4] adapted pelletized feed which improved both sulfur retention and temperature control within the system. However, later examinations of the L.C.P.R.-Process using sulfuric acid leaching[5–8] (Table I) have had difficulties in achieving satisfactory metal recoveries. The present investigation was undertaken to examine oxidation rates and to attempt to establish those factors affecting copper recoveries.

II. THERMODYNAMIC CONSIDERATIONS

Figure 1 shows an Ellingham type diagram[12] for a number of sulfation reactions in the L.C.P.R.-Process (per two moles of SO_2). Disregarding trace impurities, the process may be regarded as a five-component system. Figure 1 indicates that CaO will be sulfated in preference to iron and copper oxides at all temperatures of interest. This postulates that the presence of CaO in the roast system would result in a deficiency of SO_2 for the sulfation of other metals.

H. AHMADZAI and L-I STAFFANSSON are Research Assistant and Professor, respectively, at the Department of Theoretical Metallurgy, Royal Institute of Technology, S-100 44, Stockholm, Sweden. S. BLAIRS and B. HARRIS are both Senior Lecturers at the School of Metallurgy, The University of New South Wales, P. O. Box 1, Kensington, New South Wales 2033, Australia.

Manuscript submitted May 7, 1982.

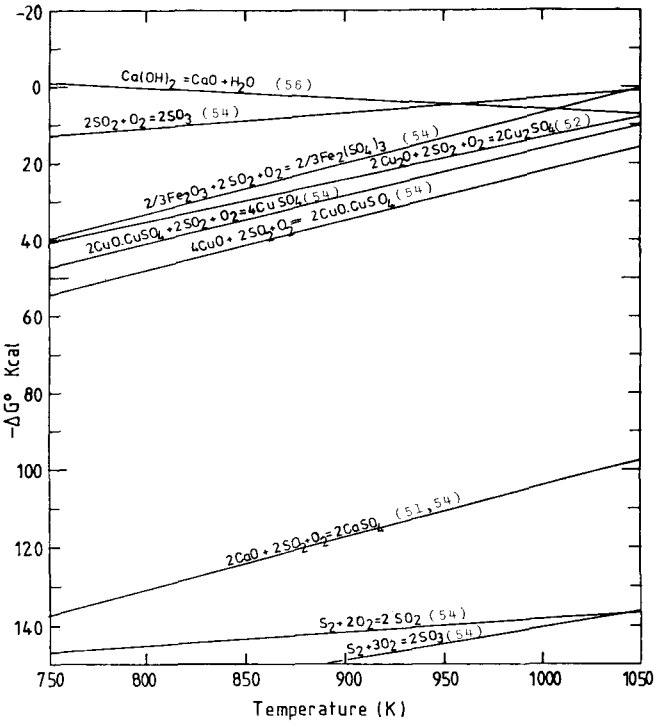

Fig. 1—Ellingham diagram for sulfation reactions in the Cu-Fe-Ca-S-O system with respect to 2 moles of SO_2. Numbers on the lines represent data sources.

Predominance area diagrams[13,14] of separate M-O-S systems may be superimposed to obtain an indication of the most stable compound of each metal.[15,16] For the L.C.P.R.-Process, Cu-Fe-Ca-S-O predominance area diagrams have been delineated from the respective M-S-O diagrams at 800 K and 1000 K (Figures 2(a) and 2(b)). It has been assumed that reactions of the individual systems are not altered by the superimposition. The standard state in the basic reactions of all substances is the pure component and for gaseous sulfur the S_2 specie at 1 atm. Data for the basic reactions and their sources are cited in Table II a, b, c. Where temperature and gas composition can be regulated, equilibrium calculations can be used to predict certain limited aspects of practical operations.[17,18] The areas marked ⊙ in Figures 2(a) and 2(b) have been calculated according to a method outlined by Kellogg[19] and were based on the composition of the Mt. Lyell concentrate as summarized in Table III. In practice, roaster gases may contain radicals S_2-S_8, O_2, SO_2, SO_3, N_2, H_2O, CO, *etc.*, but due to the

Table I. Comparison of Copper Recoveries and Sulfur Retention Achieved in the L. C. P. R. Process Using Chalcopyritic Concentrates

	Roasting		Leaching				Extraction		Retention
Ref.	Temp. K	Duration Hours	Media	Concentration gpl	Temp. K	Duration Minutes	Cu Wt Pct	Fe Wt Pct	Sulfur Retention
4	773	1	H_2SO_4	30	298	—	99	5	99
5	773	—	H_2SO_4	30	—	—	80	39	88 (a)
5	973	4	HCl	232	368	15	98	68	97 (b)
6	793	4.5	H_2SO_4	184	298	1440	87	—	83
7	793	2	H_2SO_4	184	323	120	65	—	99
8	800	—	H_2SO_4	80	353	60	67	—	99
8	873	4	H_2SO_4	80	353	60	95	10	99
10	773	4	HCl	232	368	15	99	87	98
11	973	3	H_2SO_4	60	323	180	95	13	>90

(a) Sulfur retention during fluo-solid roasting
(b) Sulfur retention during rotary-kiln roasting

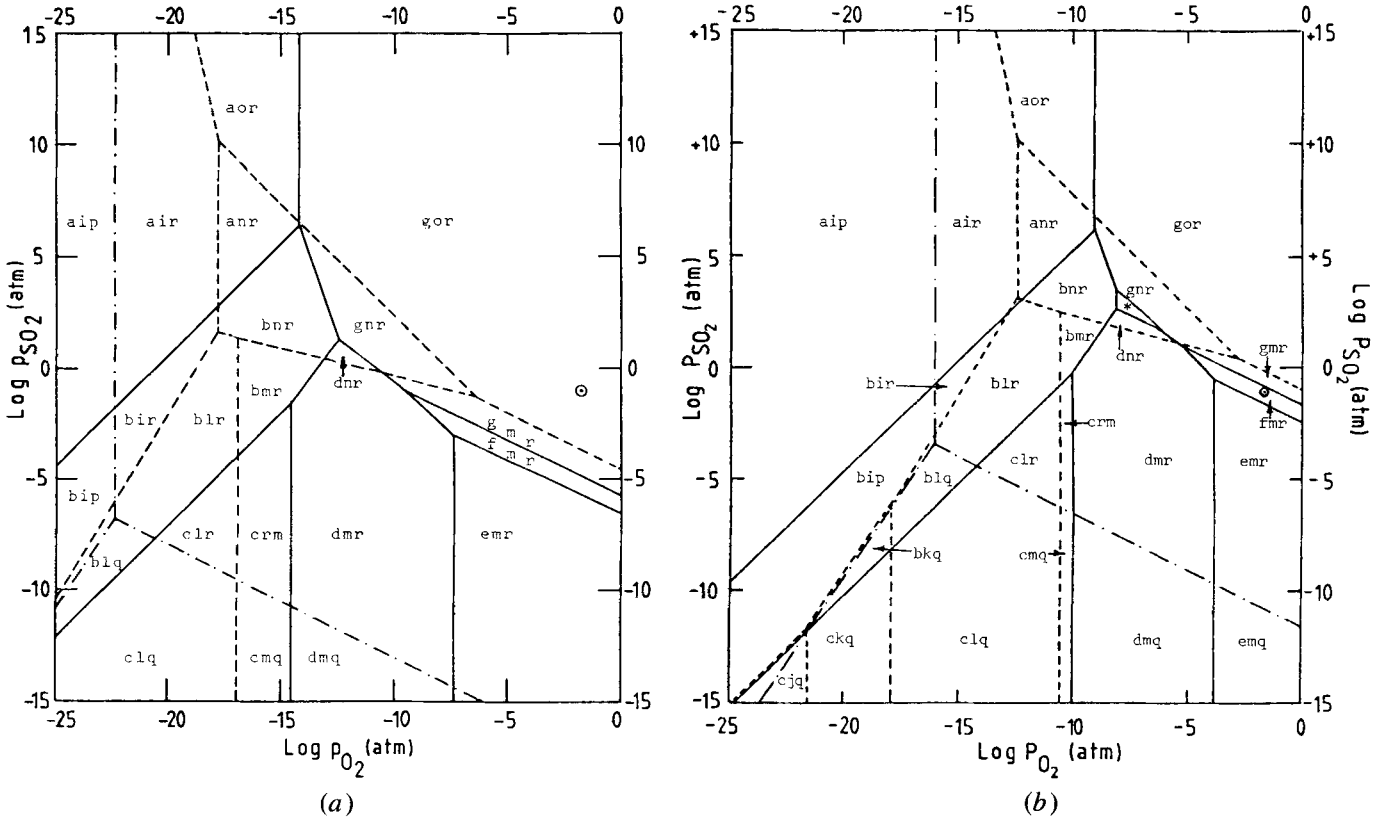

Fig. 2—(*a*) The Cu-Fe-Ca-S-O system stability domains at 800 K. Point ⊙ represents equilibrium gas composition for dead roasting Mt. Lyell concentrates. (*b*) The Cu-Fe-Ca-S-O system stability domains at 1000 K. Point ⊙ represents equilibrium gas composition for dead roasting Mt. Lyell concentrates. *Area defines stability domain for hnr. Legend: a = CuS, b = Cu_2S, c = Cu, d = Cu_2O, e = CuO, f = $CuO \cdot CuSO_4$, g = $CuSO_4$, h = Cu_2SO_4, i = FeS, j = Fe, k = FeO, l = Fe_3O_4, m = Fe_2O_3, n = $FeSO_4$, o = $Fe_2(SO_4)_3$, p = CaS, q = CaO, and r = $CaSO_4$.

oxidizing atmosphere, the important gaseous equilibrium is that of Eq. [2]:

$$2SO_2 + O_2 \rightleftarrows 2SO_3 \qquad [2]$$

However, this reaction is slow below approximately 800 K, and a catalyst is required to obtain appreciable rates.

An analysis for dead roasting conditions (marked ⊙ in Figures 2(a) and 2(b)) indicates stability of $CuSO_4$ and $Fe_2(SO_4)_3$ in the Cu-Fe-S-O system at approximately 800 K. At 1000 K, $CuO \cdot CuSO_4$ and Fe_2O_3 become the stable phases. The above conclusions, however, do not take the presence of CaO into account. Under normal roaster gas compositions, over the whole temperature range of interest, $CaSO_4$ would be the stable phase. Thus, in the Cu-Fe-Ca-S-O system, the sulfation of CaO, as shown in Figure 1, would be preferential with respect to the other metal oxides. In the L.C.P.R.-Process, oxidation roasting would therefore result in a deficiency of SO_2 for the formation of $CuSO_4$ and $Fe_2(SO_4)_3$ type compounds. Consequently, even at low roast temperatures, one may expect to find CuO, $CuO \cdot CuSO_4$, Fe_2O_3, but only diminishing amounts of $CuSO_4$ and $Fe_2(SO_4)_3$.

Table IIa. Basic Reactions in the Cu-S-O System 750 to 1000 K

Reaction	Source	$\Delta G_f^{\circ *} = a + bT^{**}$ a	b
i. $Cu_{(c)} + \frac{1}{2}S_{2(g)} \rightleftarrows CuS_{(c)}$	50	− 12476	1.010
ii. $2Cu_{(c)} + \frac{1}{2}S_{2(g)} \rightleftarrows Cu_2S_{(c)}$	51	− 31890	7.830
iii. $2Cu_{(c)} + \frac{1}{2}O_{2(g)} \rightleftarrows Cu_2O_{(c)}$	54	− 39889	16.800
iv. $Cu_{(c)} + \frac{1}{2}O_{2(g)} \rightleftarrows CuO_{(c)}$	54	− 35952	20.035
v. $2Cu_{(c)} + \frac{1}{2}S_{2(g)} + \frac{5}{2}O_{2(g)} \rightleftarrows CuO \cdot CuSO_{4(c)}$	54	−232514	120.470
vi. $Cu_{(c)} + \frac{1}{2}S_{2(g)} + 2O_{2(g)} \rightleftarrows CuSO_{4(c)}$	54	−196027	101.585
vii. $2Cu_{(c)} + \frac{1}{2}S_{2(g)} + 2O_{2(g)} \rightleftarrows Cu_2SO_{4(c)}$	52	−187128	88.339
viii. $\frac{1}{2}S_{2(g)} + O_{2(g)} \rightleftarrows SO_{2(g)}$	54	− 86586	17.515
ix. $\frac{1}{2}S_{2(g)} + \frac{3}{2}O_{2(g)} \rightleftarrows SO_{3(g)}$	54	−110023	39.765

*Kilo-calories mol^{-1}
**Accuracy ±50 cal

Table IIb. Basic Reactions in the Fe-S-O System 750 to 1000 K

Reaction	Source	$\Delta G_f^{\circ *} = a + bT^{**}$ a	b
x. $Fe_{(c)} + \frac{1}{2}S_{2(g)} \rightleftarrows FeS_{(c)}$	53	− 36020	12.650
xi. $Fe_{(c)} + \frac{1}{2}O_{2(g)} \rightleftarrows FeO_{(c)}$	54	− 64162	14.666
xii. $3Fe_{(c)} + 2O_{2(g)} \rightleftarrows Fe_3O_{4(c)}$	54	−261933	72.460
xiii. $2Fe_{(c)} + \frac{3}{2}O_{2(g)} \rightleftarrows Fe_2O_{3(c)}$	54	−193951	59.628
xiv. $Fe_{(c)} + \frac{1}{2}S_{2(g)} + 2O_{2(g)} \rightleftarrows FeSO_{4(c)}$	54	−234607	98.225
xv. $2Fe_{(c)} + \frac{3}{2}S_{2(g)} + 6O_{2(g)} \rightleftarrows Fe_2(SO_4)_{3(c)}$	54	−657557	305.720

*Kilo-calories mol^{-1}
**Accuracy ±50 cal

Table IIc. Basic Reactions in the Ca-S-O System 750 to 1000 K

Reaction	Source	$\Delta G_f^{\circ *} = a + bT^{**}$ a	b
xvi. $Ca_{(c)} + \frac{1}{2}S_{2(g)} \rightleftarrows CaS_{(c)}$	51	−129435	22.810
xvii. $Ca_{(c)} + \frac{1}{2}O_{2(g)} \rightleftarrows CaO_{(c)}$	56	−151397	24.440
xviii. $Ca_{(c)} + \frac{1}{2}S_{2(g)} + 2O_{2(g)} \rightleftarrows CaSO_{4(c)}$	51, 54	−357820	109.795

*Kilo-calories mol^{-1}
**Accuracy ±30 cal

Table III. Assay of Mt. Lyell Copper Concentrate N4

Component	Concentration, Wt Pct
Cu	24.50
Fe	31.06
S	34.62
Si	2.20
Pb, Zn, Au, *etc.*	6.84 to 7.0*
Loss on drying	0.50

*Semi-quantitative analysis

III. EXPERIMENTAL

A. *Materials*

Oxygen and air were used as oxidants, while nitrogen was used to flush the reaction system and thermobalance transducer prior to initiating an experiment.

Water vapor in the nitrogen and oxygen/air trains was removed by passage through silica gel desiccant and then through pellets of Union Carbide Type 5A molecular sieves. Carbon dioxide was removed by Ascarite. Oxygen in the nitrogen train was removed by BASF R3-11 copper catalyst at 523 K. Constant flow rates were monitored using calibrated capillary flowmeters. Dibutyl phthalate was used as the manometric fluid. The gases were mixed in a chamber filled with ceramic saddles.

The chalcopyritic concentrate was provided by the Mt. Lyell Mining and Railway Co. from their Mt. Lyell (Tasmania) operations. The concentrates particle size distribution, as measured by Endecott Metric Test Sieves, is depicted in Table IV.

Univar AR Grade calcium hydroxide (100 wt pct passing Endecott Test Sieve 400 (38 μm)) was used for the larger part of the experimental program. Hydrated lime as obtained from Blue Circle Southern Cement Ltd. (Berimma Works) was also mixed with the concentrate to examine system response using only commercial materials. The chemical composition of the Blue Circle Southern Cement Ltd. hydrated lime is listed in Table V and its particle size distribution in Table VI. Stoichiometric amounts of hydrated lime and concentrate were blended and pelletized in a pellet press at 64.42 ± 0.71 MPa.

A commercial Heraeus Type 1 vertical tube furnace was used to heat the pellets. Temperature control (±5 K) was achieved using a Smith Series 6 potentiometric temperature controller and a Pt/Pt-10 pct Rh control thermocouple. A constant temperature zone of approximately 5 cm length was duly marked under dynamic conditions. The reaction tube was constructed of 39 mm I.D. transparent silica tube. To monitor the progress of the reaction, a Kyowa Type 120-T-10B resistance strain gauge transducer was employed. To prevent thermal segregation, an isothermal system with thermal baffles and air cooling was constructed around the transducer housing. Transducer output voltages were recorded on a Northrop Leeds Speedomax H-AZAR recorder.

Table IV. Size Analysis Mt. Lyell Copper Concentrate

Std. Sieve Designation	Microns μm	Wt Pct Retained
+ 50	+300	0.80
+ 70	−300 + 210	1.55
+100	−210 + 150	1.46
+140	−150 + 105	4.45
+200	−105 + 75	20.77
+270	− 75 + 53	27.72
+400	− 53 + 38	30.89
−400	− 38	12.36

Table V. Assay of Blue Circle Southern Cement Ltd. (Berrima) Hydrated Lime

Component	Concentration, Wt Pct
CaO	73.30
Al_2O_3	0.45
MgO	0.26
Fe_2O_3	0.18
SiO_2	0.89
Loss on ignition	24.50

Table VI. Size Analysis Blue Circle Hydrated Lime

Std. Sieve Designation	Microns μm	Wt Pct Retained
+100	+150	1.19
+140	−150 + 105	4.87
+200	−105 + 75	8.77
+270	− 75 + 53	21.50
+400	− 53 + 38	42.64
−400	− 38	21.03

B. *Experimental Procedure*

The pellets were measured using a micrometer and weighed on a precision microbalance prior to each roasting. A pellet was then attached *via* its platinum suspension hook to a silica fiber and thence to the transducer. The transducer housing was subsequently lowered onto the reaction tube and the assembly was flushed with N_2. Once the system had thermally stabilized in the isothermal enclosure, the tube furnace was raised to allow complete dehydration of the pellet. On the completion of dehydration, predetermined mixtures of air/O_2-N_2 were introduced into the reaction vessel. The progress of the reaction was monitored gravimetrically and by analysis of the exit gases. Due to short residence time and absence of catalytic agents, SO_2 predominates. The SO_2 content of the exit gases was determined using standard iodine/iodate method and starch indicator.

The roasting sequence was terminated and "quenched" by reintroduction of N_2 and lowering the furnace. The cold reacted pellet was subsequently reweighed, its dimensions remeasured, and then sectioned for further micro-and-macro examination.

IV. RESULTS

A typical mass gain curve for a cylindrical compact (1 cm × 1 cm) reacted at 773 K is shown in Figure 3. Results have been evaluated in terms of oxygen mass transfer. Sections from partially reacted pellets were observed to remain topochemical throughout the duration of a run

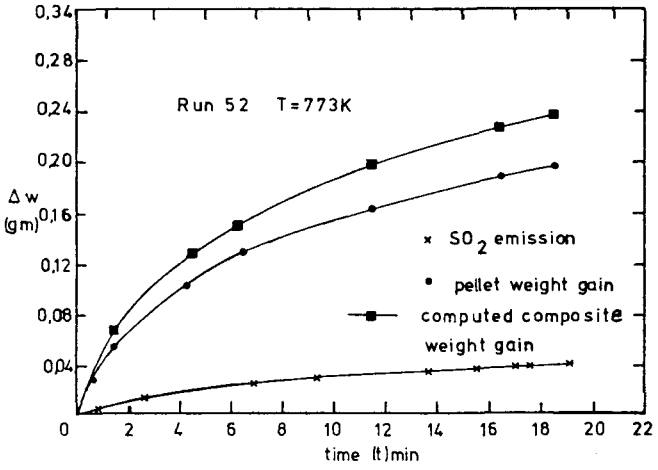

Fig. 3—Oxidation curve for the roasting of a single pellet at G = 0.0015 gm/cm^{2}s ($\dot{v}_{303\,K}$ = 15 cm^3/s) at T_f = 773 K.

(Figure 4, page 599). The sample mass and position of the interface were related by:

$$r^* = \frac{r_i}{r_o} = \left[\frac{m_f - m_t}{m_f - m_o}\right]^{1/3} \qquad [3]$$

Progressively increasing air flowrates (21 pct oxygen) were employed to establish the range of flow necessary to overcome the starvation effects and to minimize boundary layer resistance. No significant change in initial rate was observed beyond G = 0.0015 gm/cm^2 second. All subsequent runs were investigated at this flowrate. Effect of temperature was evaluated at 753 K, 773 K, and 873 K. Composite weight gain data were nonlinearly regressed and the resulting best fit polynomial differentiated to obtain the slope at t = 0 (Figure 5). Values obtained were equated by the appropriate stoichiometric factor, and the initial reaction rates are listed in Table VII. After approximately 1.5 minutes the reaction front advances sufficiently into the pellet for structural parameters to become significant. As the reaction front recedes, the rate of SO_2 evolution decreases markedly (Figure 6) and is accompanied by a change in pellet mass gain curve indicating a change in controlling parameters. Pellets were normally compacted at approximately 64 ±8 MPa. This variation in compaction pressures resulted in varying pellet densities and porosities which in turn affected the effective diffusivity of oxygen into the pellet. Run 48 compacted at approximately 170 MPa and runs compacted at approximately 64 MPa are illustrated in Figure 7. The variation in effective diffusivity is summarized in Table X below.

Table VII. Composite Reaction Rates ($t \rightarrow 0$) for Oxidation of Lime-Concentrate Pellets with Varying Furnace Temperatures. Analyses in Terms of Oxygen Transfer.

Experimental Run	Temperature T_f, K	$\dot{v}_{303\,K}$ cm^3/sec	Composite Rate $\dot{n}$ (E 06)* moles/sec
43	753	15	29.01
73	773	15	30.38
72	873	15	22.40

*$\dot{n}E$ 06 refers to $\dot{n} \times 10^6$

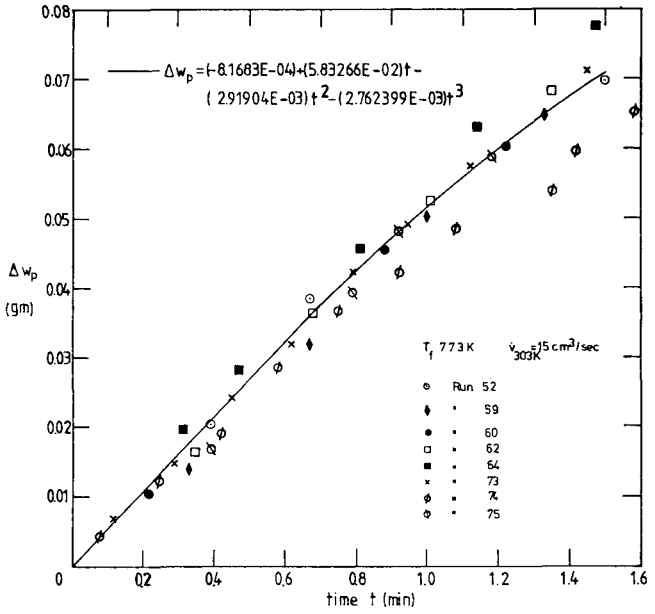

Fig. 5—Initial composite weight gains for the oxidation of lime-concentrate pellets. Equation of the line to fit Run 73.

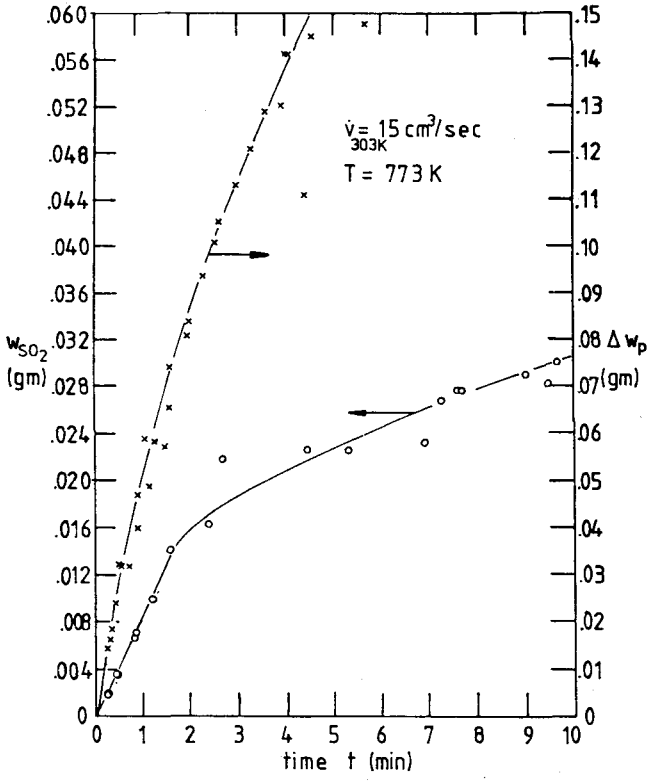

Fig. 6—Effect of structure on the oxidation rate. A marked decrease in the evolution of SO_2 is noted once the interface recedes from the surface of the pellet.

Increase of temperature from 753 K to 773 K had only a minor influence on the oxidation rate. At 873 K, however, due to massive sintering, a decrease occurs. The rate of sulfur dioxide evolution increases slightly with temperature, and the overall sulfur retention at 773 K was approximately 92 wt pct using Univar AR Grade lime and approximately 93 wt pct using Blue Circle hydrated lime. Leaching studies

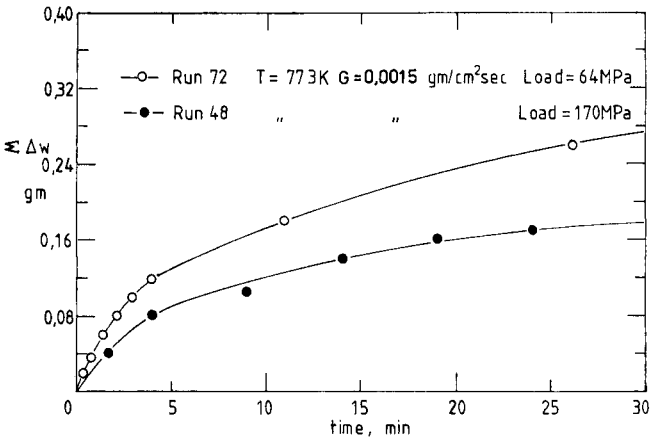

Fig. 7—Effect of varying compaction load on the oxidation rate of lime-concentrate pellets.

on calcines from the 773 K roasts were compared with earlier investigations.[4-6,11] The results are depicted in Figure 8. Roasted pellets were leached using standard procedure.[20] 16 wt pct solid slurries were prepared from crushed calcines (100 wt pct < 1680 μm) and 98 gram per liter H_2SO_4 (1 M H_2SO_4). Leaching temperature was regulated at 358 K, and the slurries were continuously agitated. Sample solutions were subsequently analyzed for Cu and Fe by an atomic absorption spectrophotometer.

The maximum extraction achieved after 210 minutes was 80.4 wt pct copper. To confirm presence of the product phases predicted thermodynamically and to examine the factors resulting in low copper recoveries, X-ray powder patterns of the materials removed from the periphery and core of a completely reacted pellet were obtained using Debye Scherrer techniques with a Philips PW 1024 114.83 mm camera and iron-filtered Co K_α radiation. Observed diffraction lines were compared with lines from the ASTM files.[21] Thermodynamic computations above indicated that the major phases should be CuO, Fe_2O_3, and $CaSO_4$ with diminishing quantities of CuO · $CuSO_4$ and $CuSO_4$. That the major phases are CuO, Fe_2O_3, and $CaSO_4$

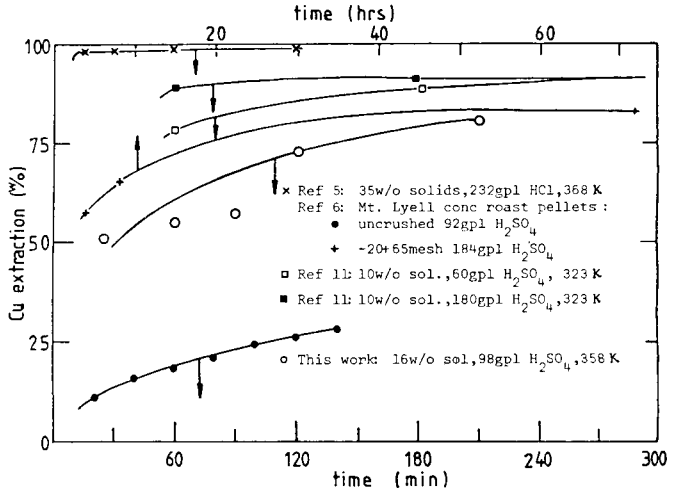

Fig. 8—Leaching of lime-concentrate roasted pellets under agitated slurry conditions of 98 gpl H_2SO_4, 16 wt pct solid density, and 358 K. Extraction after 210 min = 80.4 wt pct.

was confirmed by the X-ray diffraction analyses. Some CuO · $CuSO_4$ was present but no distinguishable quantities (>5 wt pct) of $CuSO_4$ were observed either in the periphery or the pellet core. Phases resulting from low oxygen potential, *e.g.*, Fe_3O_4, CaS, $Cu_{1.96}S$, and $FeSO_4$, were found in the core. There was some disagreement of the experimental "d" spacing of $FeSO_4$ with those reported in the ASTM compilation, but they conformed closer with the values reported recently by Skeaff *et al.*[22] Copper and calcium ferrites were observed in both the core and periphery, and some unreacted high temperature (773 K) Cu_2S and $Cu_{1.98}S$ was also observed.

The exothermic nature of the roast reaction was followed by placing the hot junction of a thermocouple inside a pellet and by a separate one positioned in close proximity to the pellet surface within the gas phase. Figure 9 depicts the temperature profile during a reaction. For runs at 773 K, the pellet and the external temperatures, respectively, peaked at 975 K and 840 K (approximately) after approximately 1.5 minutes from the inception of oxidation. The internal temperature history could be reproduced to within ±2 pct, but the response of the external thermocouple was influenced by a minor change in the location of the hot junction relative to the reacting pellet. In the majority of experiments, the external thermocouple was placed approximately 1.5 mm from the pellet. As in the beginning of the reaction the temperature at the interface of the pellet is essentially equal to that of the furnace, all initial rates have been analyzed in terms of isothermal conditions. For rates other than at inception, account has been taken of the temperature at the reaction interface.

A. *Evaluation of Mass Transfer to the Pellet*

Figure 10 represents behavior obtained by assuming that mass transfer through the product layer is controlling whereby:

$$3 - 3(1 - F)^{2/3} - 2F = 6D_{\text{eff}} \cdot \frac{\Delta P t}{RT\rho r_0^2} \qquad [4]$$

This assumption is supported by the linearity of plots in Figure 10. Reciprocal sigmoidal curves obtained on assuming interfacial control suggest that steps other than chemical control at the interface are important.

To determine the importance of convective mass transport, evaluated and observed initial rates were compared. Convective mass transfer across the gas boundary layer was evaluated using the Ranz Equation:[24]

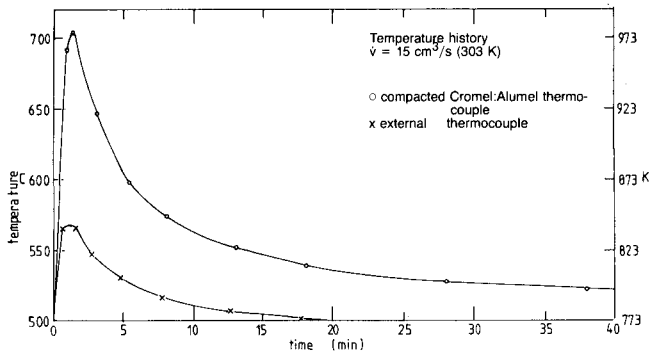

Fig. 9—Temperature variation of a reacting lime-concentrate pellet. Furnace temperature T_f = 773 K.

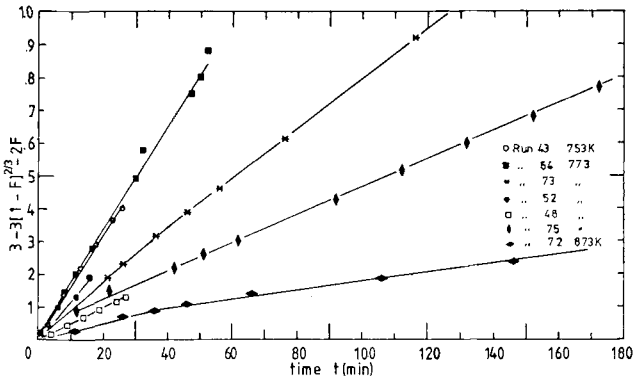

Fig. 10—Experimental plot of rate data plotted with respect to the shell diffusion model.

$$\mathrm{Sh} = 2 + 0.6(\mathrm{Re})^{1/2}(\mathrm{Sc})^{1/3} \quad [5]$$

The density of air was computed from the formula:[25]

$$\rho_{\mathrm{Air},T} = 1.2929\frac{(273.13)}{T} \quad [6]$$

and the diffusivity of O_2-N_2 mixtures by the method[26]

$$D_{12} = \frac{0.001858T^{3/2}[(M_1 + M_2)/M_1M_2]^{1/2}}{P\sigma^{*2}_{12}\Omega_D} \quad [7]$$

Table VIII lists the convective mass transfer coefficients as evaluated for the investigated conditions. Since the equilibrium partial pressure is very small, the observed and calculated convective mass transfer coefficients were correlated by Eq. [8]:

$$\dot{n} = \frac{dw}{dt}\cdot\frac{1}{32} = \frac{\alpha 4\pi r_o^2}{\mathrm{R}T_b}\cdot P_{\mathrm{O}_2,b} \quad [8]$$

Due to the inherent geometry of the system, mass transfer coefficients evaluated from Eq. [5] may have slight inaccuracies.[27] Table VIII also tabulates quantitatively the fraction of resistance that is due to mass transfer (ϕ_{MT}):

$$\phi_{MT} = \frac{\dot{n}_{in,ob}}{\dot{n}_{in,th}} \quad [9]$$

At 773 K, the theoretical rate is 33.28E-06* mol per second and $\phi_{MT} = 0.91$.

*mE-06 stands for mx10^{-6}.

B. *Evaluation of Overall Heat Transfer*

The significance of heat transfer was evaluated by approximating the furnace to an enclosure whose surface area is large with respect to the sample. Due to absence of data on the emissivity of an oxidized lime concentrate pellet, it was assumed that the sample behaves as a grey body. The overall heat transfer coefficient (h_{ov}) was evaluated according to the equation:

$$h_{ov} = h_{rad} + h_{conv} \quad [10]$$

where[28]

$$h_{rad} = E_{12}\sigma(T_1^3 + T_1T_2^2 + T_2^2T_1 + T_2^3) \quad [11]$$

and

$$E_{12} = \frac{1}{(1/E_1 + 1/E_2) - 1} \quad [12]$$

The convective heat transfer coefficient was evaluated from the Nusselt-Prandtl correlation analogy to Eq. [5]:

$$\mathrm{Nu} = 2.0 + 0.6(\mathrm{Re})^{1/2}(\mathrm{Pr})^{1/3} \quad [13]$$

Assuming that all heat transferred to the reaction front is absorbed by the reaction and that steady state conditions prevail, heat transfer to the reaction front can be represented by an equation for the conservation of heat at the reaction front:[29]

$$\dot{q} = -\Delta H_r\dot{n} \quad [14]$$

and

$$\dot{q} = \frac{4\pi k(T_r - T_g)}{\frac{1}{r_i} - \frac{1}{r_o} + \frac{k}{h_{ov}r_o^2}} \quad [15]$$

Eqs. [14] and [15] can be rearranged to yield:

$$\dot{n} = \frac{4\pi kr_o(T_r - T_g)}{\Delta H_r\left[(1/r^*) - 1 + \frac{k}{h_{ov}r_o}\right]} \quad [16]$$

The importance of heat transfer may be evaluated by substituting the relevant values into Eq. [16] and comparing them with the observed rate at the respective time and degree of fractional oxidation.

The enthalpy of reaction considered for evaluation of heat transfer effects was that for the oxidation of chalcopyrite and lime based on one mole of oxygen according to the reaction:

$$\tfrac{4}{17}\mathrm{CuFeS_2} + \tfrac{8}{17}\mathrm{CaO} + \mathrm{O_2} \rightleftarrows \tfrac{4}{17}\mathrm{CuO} + \tfrac{4}{34}\mathrm{Fe_2O_3} + \tfrac{8}{17}\mathrm{CaSO_4} \quad [17]$$

In the absence of data for the thermal conductivity of oxidized lime-concentrate pellets, the conductivity was estimated from the experimental results according to the method outlined by Hills.[30] Thermal conductivity estimated in the

Table VIII. Experimental and Calculated Initial Reaction Rates and the Importance of Gas Film Boundary Resistance

Temp. K	Mass Flux G, gm/cm² sec	Experimental, This Work $\alpha_{i,ob}$ cm/sec	Experimental, This Work $\dot{n}_{i,ob}$ E 06 mol/sec	Theoretical, Equation 5.0 α cm/sec	Theoretical, Equation 5.0 $\dot{n}$E 06 mol/sec	Experimental, Ref 32 $\alpha_{i,ob}$ cm/sec	Experimental, Ref 32 $\dot{n}_{i,ob}$ E 06 mol/sec	$\phi_{MT} = \frac{\dot{n}_{i,ob}}{\dot{n}_{i,th}}$
753	0.0015	2.72	29.01	3.08	32.88	—	—	0.88
773	0.0015	2.92	30.38	3.20	33.28	—	—	0.91
873	0.0015	2.43	22.40	3.87	35.64	—	—	0.63
723	0.0020	—	—	2.60	38.24	1.79	26.33	0.69
773	0.0020	—	—	2.90	39.89	1.92	26.41	0.66
873	0.0020	—	—	3.52	42.87	2.29	27.89	0.65

above manner is listed in Table IX. Due to experimental scatter, evaluation of the effective thermal conductivity has an accuracy of approximately ±45 pct. Thermal conductivity varies with the temperature, but due to the error involved has been reported only to a single significant value. Effect of thermal resistance, however, is minor in that an error of 45 pct results in an inaccuracy of ±3 pct in the predicted theoretical rate. Table IX compares observed and postulated reaction rates. For the range of conditions encountered, the observed reaction rates are greater than those predicted theoretically. This emphasizes the insignificance of heat transfer in the oxidation of lime-concentrate pellets.

C. *Evaluation of the Effective Diffusion Coefficient*

Assuming that both boundary layer diffusion and diffusion through porous product layer contribute toward effective control of the rate, the total mass transfer rate can be represented by the form:

$$\dot{n} = \frac{4\pi D_{eff}\Delta P}{RT_g\left(\frac{1}{r_i} - \frac{1}{r_o} + \frac{D_{eff}}{\alpha r_o^2}\right)} \qquad [18]$$

Since K_{Eq} for the oxidation reaction is very large, Eq. [18] may be rearranged to the form:

$$\frac{P_{O_2 b}}{\dot{n}} = \frac{RT_g}{4\pi D_{eff} r_o}\left(\frac{1}{r^*} - 1\right) \cdot \frac{RT_g}{4\pi\alpha r_o^2} \qquad [19]$$

A plot of $P_{O_2 b}/\dot{n}$ *vs* $(1/r^*) - 1$ results in a straight line whereby both the convective mass transfer as well as the effective diffusion coefficients may be evaluated from the intercept and slope, respectively. Since in the early stages of the reaction, resistance due to diffusion through the product layer is diminutive, the curve has a different value as compared with the later stages when reactant oxygen has to diffuse through the product. This is illustrated in Figures 11(a) and 11(b) which depict, respectively, the initial and the overall segment of the reaction. The effective convective mass transfer coefficient as evaluated from the initial plot (Figure 11(a)) resulted in $\alpha = 2.98$ cm per second which compares well with that obtained more directly from the tangent at $t \rightarrow 0$ (Figure 5), whereby $\alpha = 2.92$ cm per second. All the experimental effective diffusivities were evaluated from the overall plots of $P_{O_2 b}/\dot{n}$ *vs* $f(r^*)$ by disregarding the initial few seconds of the run. Table X tabulates the observed effective diffusivities at various temperatures and compactions.

V. DISCUSSION

Reaction mechanisms cannot be established by analyses of curves of $f(F)$ *vs* time. Nevertheless, relative insignificance of overall interface control is emphasized by distinct sigmoidal shapes of plots of $(1 - F)^{1/3}$ *vs* time and by the relative linearity of the fractional oxidation function *vs* time assuming sole diffusion control, *i.e.*, Figure 10.

For interface control to be significant, the observed oxidation rates would have to be much smaller than those evaluated theoretically for the set conditions. The bulk air mass velocity (G) employed for roasting was 0.0015 gm/cm^2 s. This was sufficiently high for starvation control to be absent. On the basis of established theory, such high flowrates ($Re_p = 4.1$) would also result in insignificant boundary layer thickness and consequently, resistance to convective mass transport may be ignored. In a separate evaluation of the significance of boundary effects, a reacting pellet was suspended in close proximity to the reactor wall (approximately 0.5 to 1.0 mm). This technique varies system geometry so that convective mass transfer to the interface is modified. If boundary layer resistance is significant, change in the shape of the interface should be observed.[27] In a recent analysis by Hills,[31] however, it has been shown that mass transfer effects may be ignored only if the value calculated using Eq. [9] is extremely small. In the present case, mass transfer appears to account for approximately 90 pct of the resistance.

The mass velocity employed in the present investigation ($G = 0.0015$ gm/cm^2 s, $Re_p = 4.1$, $Sh = 3.1$) was approximately equal to the velocity employed in an earlier study by Haung and Bartlett[32] ($G = 0.002$ gm/cm^2 s).

Table X. Tabulation of the Observed Effective Diffusivity in Oxidized Lime-Concentrate Pellet under Various Temperatures and Compaction Loads

Designation	Run 43	Run 73	Run 72	Run 48
Temperature, K	753	773	873	773
Air mass velocity G gm/cm^2 sec	0.0015	0.0015	0.0015	0.0015
Compaction load, MPa	63.40	64.42	64.42	170
Observed effective diffusivity cm^2/sec	0.065	0.038 0.233[§]	0.018	0.017

[§]Effective diffusivity evaluated from initial segment of plot (Fig. 11(a)). Corresponding convective mass transfer coefficient $\alpha = 2.98$ cm/sec.

Table IX. Evaluation of the Importance of Heat Transfer to the Reaction Front

Time, min	T_r, K	T_g, K	$(1/r^*) - 1$	$-\Delta H_r$ kJ/mol	k_p W/mK	Theoretical $h_{ov,r}$ W/m^2 K	Theoretical $\dot{n}$ E 06 mol/sec	Observed $\dot{n}$ E 06 mol/sec
0	—	773	—	—	—	110.29	—	—
0.67	925	840	0.037	775.530	0.6	143.27	4.72	26.41
1.50	976	840	0.072	776.391	0.6	155.99	7.85	14.64
4.37	890	807	0.151	774.940	0.6	135.06	3.88	7.34
6.50	859	795	0.193	774.417	0.6	128.13	2.76	5.47
11.50	831	781	0.292	773.944	0.6	122.13	1.91	4.11
16.50	816	776	0.380	771.885	0.6	119.02	1.41	2.55

Run 52

$\dot{n}_i$(0-1.0 min) = $(dw)/(dt) \cdot 1/32 = 1.823E\text{-}03 - 182.438E\text{-}06t - 258.969E\text{-}06t^2$ moles/min

$\dot{n}_{ov}$(1.5-16.5 min) = $1.325E\text{-}03 - 366.563E\text{-}06t + 49.375E\text{-}06t^2 - 2.978E\text{-}06t^3 + 64.875E\text{-}09t^4$ moles/min

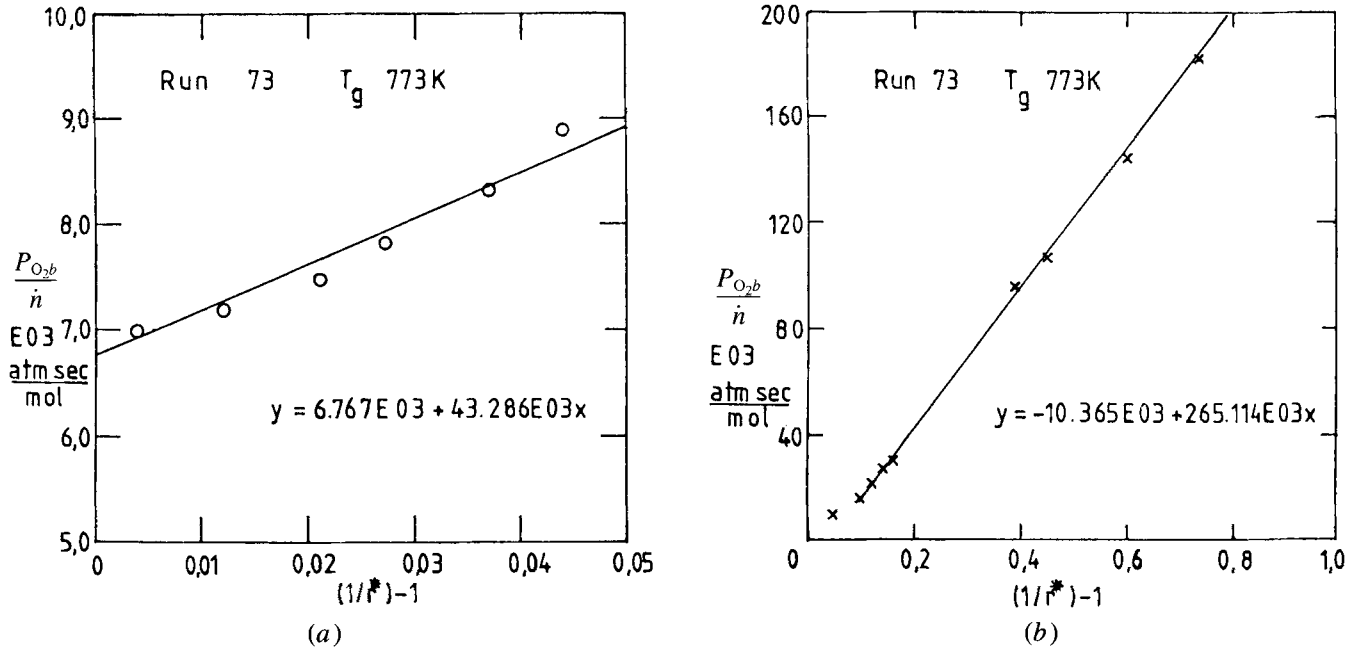

Fig. 11 — (*a*) Plot of $P_{O_2 b}/\dot{n}$ *vs* function of fractional oxidation for the initial stages of Run 73. (*b*) Plot of $P_{O_2 b}/\dot{n}$ *vs* function of fractional oxidation for the overall stage of Run 73 ignoring the initial stage.

Haung and Bartlett reported that pellet roasting was boundary layer controlled in the initial stages of reaction and diffusion controlled through the product layer in the later stages of the reaction. Evaluation of their data, Table VIII, indicates that mass transfer resistance amounts to approximately 68 pct of the total resistance. The present results are in agreement with their analysis in that the roasting appears to be boundary layer controlled in the initial stages and mixed gas boundary layer-product layer diffusion controlled for the overall rate.

With approximately 90 pct of the total resistance being attributed to boundary layer diffusion, the observed initial reaction rates do not represent the intrinsic chemical rate for the oxidation of lime-concentrate pellets. An added complication is that initially, the reaction stoichiometry differs from that represented by Eq. [20]:

$$CaO + SO_2 + O_2 \rightleftarrows CaSO_4 \qquad [20]$$

During the initial stages of oxidation, the residence time of SO_2 at the pellet periphery is insufficient for Eq. [20] to go to completion. This is evident from the rate of SO_2 evolution at the inception of the reaction (Figure 6). As the interface recedes into the pellet with progress of time, the rate approaches asymptotically the stoichiometry represented by Eq. [20]. Also, the reactivity of lime and concentrate as derived from differing source materials varies,[33,34,35] and initial reaction rates would be influenced by such variations.

Diffusional effects due to the product layer are difficult to eliminate even by use of very thin pellets,[36] and as the reaction interface moves below the surface, porosity influences the reaction rate. Where sintering occurs, it has a marked effect on porosity. It reduces the area available for diffusion and retards reaction rates. This phenomenon is emphasized by pellet roasting at 873 K (Table VII). While rates rise marginally with temperature over the range 753 K to 773 K, a marked drop occurs at 873 K. Had interface control been of significance, the "apparent" rate would have increased. Mt. Lyell concentrates have been reported as showing agglomeration tendencies during low temperature (approximately 953 K) oxidation roasts.[37] In the present study, marked sintering was observed during oxidation at 873 K and to a lesser extent at 773 K (Figures 12(a-d)).

At 773 K the times for completion of reaction varied from approximately 60 minutes to 220 minutes. This is ascribed to variations in individual compaction loads. Pelletization by the punch and die method also results in an uneven distribution of compacting pressure and induces densification over a peripheral thickness of approximately 138 μm (Figure 13). This peripheral densification results in reduced porosity and varied diffusivity with respect to the bulk of the material.

The marked deterioration of the "overall" rate at 873 K (Figure 10) is also partly attributable to change in the molar volumes of the reactants and products. Figure 14 depicts the position of the reaction interface at 873 K after 210 minutes and represents a fractional oxidation of approximately 85 pct. In comparison, at 773 K 100 pct oxidation is achieved in 60 minutes. Incomplete solid conversion after prolonged reaction is often attributed to structural changes in the reactants and products. The reaction between SO_2, O_2, and limestone has been described in these terms.[38]

Figures 15(a), (b), and (c) show scanning electron micrographs of the fractured surfaces of the reacted zones from 773 K and 873 K roasts, respectively. Densification and reduction of porosity is marked, especially for the 873 K roast. That the effect of sintering is more pronounced at 873 K than at 773 K is clearly visible from Figure 12(d). This densification reduces effective diffusivity. The consequential oxygen potentials are lowered and these alter the reaction stoichiometry. Thermodynamically, the oxidation

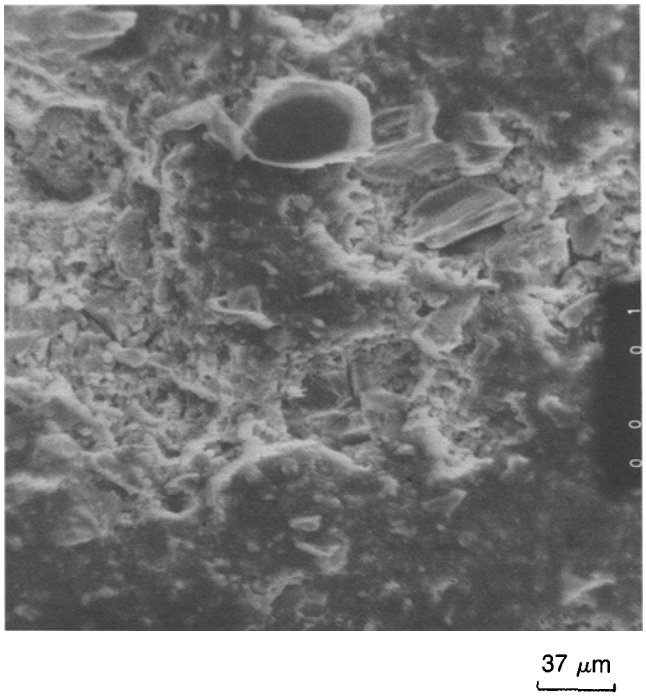

(a)

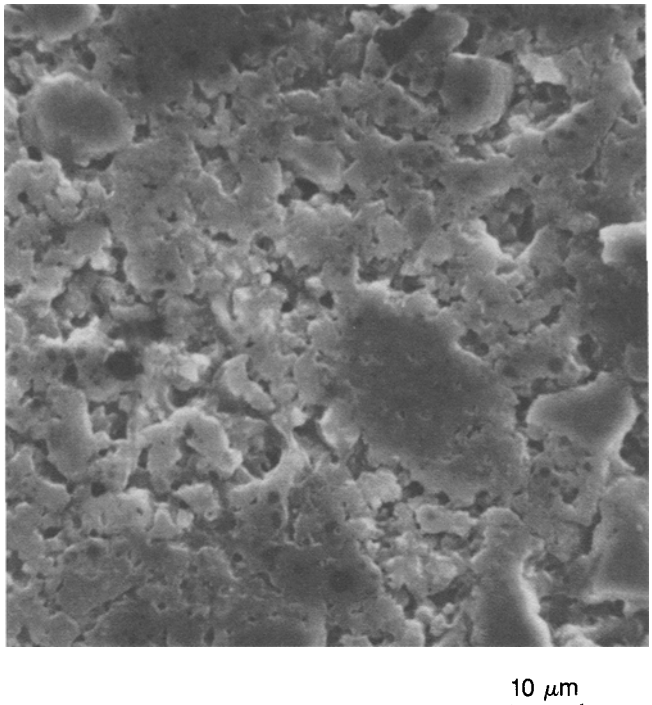

(b)

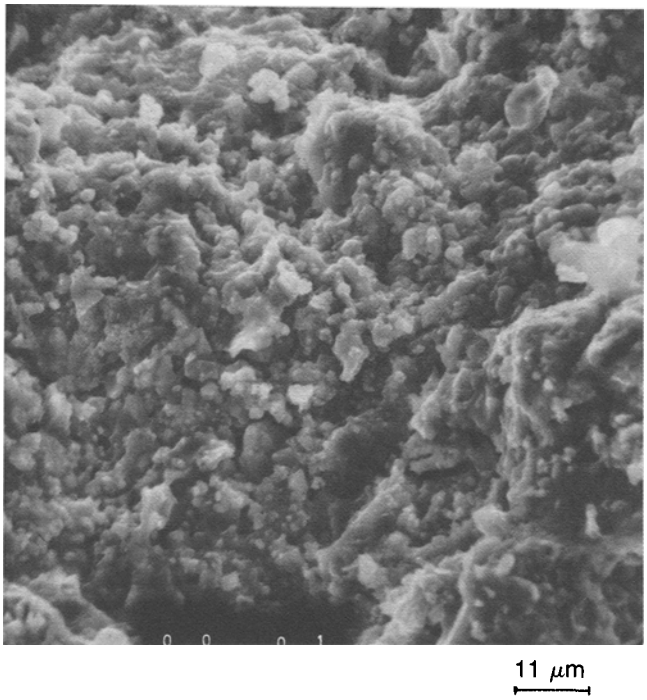

(c)

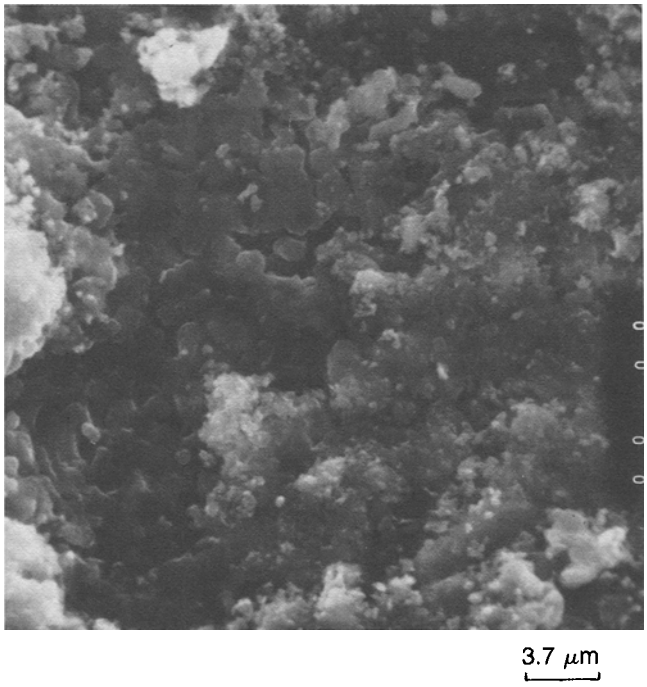

(d)

Fig. 12—(*a*) Compacted pellet prior to reaction. (*b*) Sintering effects at 773 K. The scanning electron micrograph depicts a polished surface from an unreacted zone in a pellet reacted at 773 K. (*c*) Sintering effects at 773 K. Fracture surface of an unreacted zone of a pellet. (*d*) Sintering effects at 873 K. Micrograph of a fracture surface of an unreacted zone showing a more pronounced sintering phenomenon as compared with that at 773 K (c). The decrease in pore size is significant.

of iron sulfides is more favorable than copper sulfides. An electron microprobe across a partially reacted copper-iron-sulfide particle indicated that reaction at the interface appears to proceed with iron diffusing out of the matrix of the Cu-Fe-S particle faster than copper. This results in a relatively higher concentration of copper in the Widmanstätten type yellow colored phase in Figure 16. This Widmanstätten type structure appears to recede in a topochemical manner and transforms to a greyish phase. According to Thornhill and Pidgeon,[39] the interface consists of diginite ($Cu_{2-x}S$, $Cu_{1.8}S$) which allows rapid inward diffusion of copper and outward diffusion of iron. The diginite-chalcopyrite interface advances by continued displacement of iron with copper until the entire kernel is converted to the diginite phase.

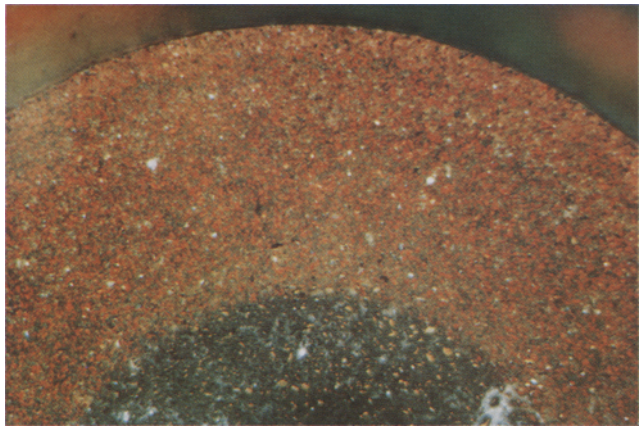

Fig. 4 — Photomicrograph of a partially reacted lime-concentrate pellet under polarized light. Roast temperature 773 K.

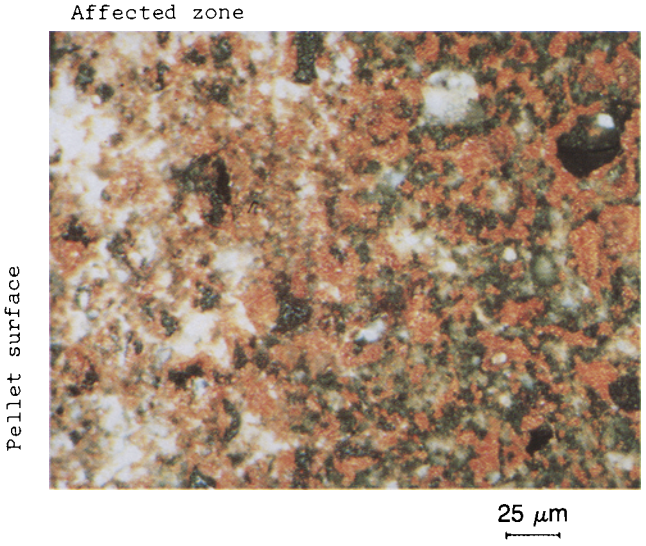

Fig. 13 — Varying structure due to uneven distribution of forces during compaction in a cylindrical die. The left side shows densification of the pellet periphery relative to the bulk structure shown on the right-hand side. Note also the black unoxidized copper-iron-sulfide particles.

Fig. 14 – Interface of a lime-concentrate pellet reacted at 873 K for 210 mins at $G = 0.0015$ gm/cm^2 s. Two interfaces, *i.e.*, the outer dark brown reaction zone and the lighter inner reacted zone, are clearly visible.

Fig. 16 – Micrograph of a copper sulfide particle at the interface of a pellet oxidized at 773 K. The bright yellow phase is copper rich and recedes as the reaction progresses. The oxidation products are distinguishable by the reddish tone.

The detailed stepwise kinetics and sequence of oxidation of Cu-Fe-S is complex and has not been considered here. Preferential oxidation of iron sulfide at the interface of each massive Cu-Fe-S grain to magnetite (Fe_3O_4) or hematite (Fe_2O_3) is dependent on the local oxygen potential. In the Cu-Fe-Ca-S-O system (Figures 2(a) and 2(b)) it is apparent that provided P_{SO_2} remains below 1 atmosphere (760 torr), the oxidation of iron sulfide would result in Fe_3O_4 prior to Fe_2O_3. If the oxygen potential remains low, Fe_3O_4 would remain stable.

For the case where one mole of $CuFeS_2$ forms Fe_3O_4 and Cu_2S, the theoretical volume is 5 pct larger than for the formation of Fe_2O_3 and CuO partly because Fe_3O_4 has a larger molar volume than Fe_3O_4. Examination of the pellet dimensions prior to and after oxidation at 873 K (Figure 14) indicated a 7.5 pct increase (approximately 0.4 pct increase at 773 K).

Macroscopic examination of the reaction zone from an 873 K roast (Figure 14) indicated two distinct reaction zones. Visually, the outer zone resembles that of the reacted zone at 773 K.

The marked variation of pellet volume, mass, and reaction zone at 873 K indicates a major change in the reaction stoichiometry compared with that at 773 K. X-ray powder diffraction patterns from the periphery of a pellet roasted at 773 K showed no evidence of phases characteristic of low oxygen potentials in the reaction system (*e.g.*, Fe_3O_4, Cu_2S, Cu_2O, $FeSO_4$). Powder patterns show, however, the occurrence of these phases in the pellet core where the oxygen potential is lower due to diffusional resistance.

At 873 K due to sintering, oxygen potential at the surface is lowered from the inception of roasting. Formation of

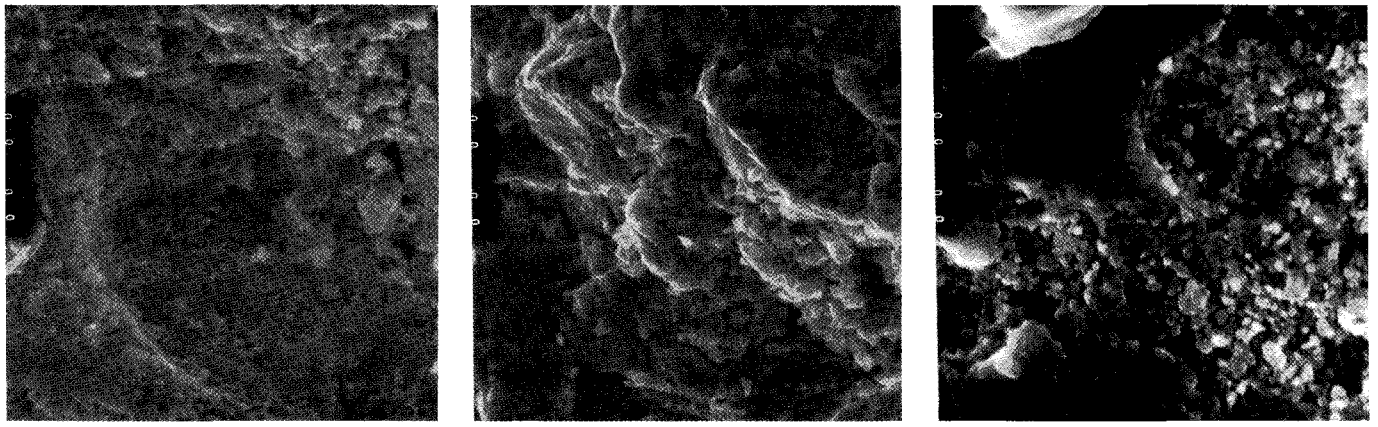

Fig. 15—(*a*) Scanning electron micrograph of the fracture surface of the reacted zone from a pellet roasted at 773 K. (*b*) Micrograph of the fracture surface of the reacted zone from a pellet roasted at 873 K. Note the lack of large pores compared to that of (a). (*c*) Fracture surface of a reacted zone from an 873 K roast. A decrease in porosity is noticeable compared to that of the sintered unreacted zone depicted in Fig. 12(d).

Fe_3O_4 and $CaSO_4$ further increases the molar volume of the system and causes additional pellet densification resulting in an incomplete pellet roast as observed at 873 K. The outer segment of the reaction zone of pellets from 873 K roasts resembles that of the 773 K roasts because of greater oxygen access with extended times. That a similar phenomenon does not occur at 773 K is essentially due to the less pronounced effects of sintering on the reactant solid.

A. *Leaching of Lime-Concentrate-Pellet-Roast Calcines*

While Figure 8 shows an improvement of efficiency for leaching of calcines obtained from Mt. Lyell concentrates, the maximum copper extractions obtained are still low as 98 to 99 wt pct extraction is desirable. Failure of sulfuric acid leaching to achieve high copper extraction from calcines in roast-leach processes has usually been ascribed to either formation of copper ferrites and/or copper entrapped as unreacted copper sulfide grains. The copper ferrites of interest are $CuFe_2O_4$ and $CuFeO_2$. $CuFe_2O_4$ is insoluble in dilute sulfuric acid and $CuFeO_2$, although apparently soluble compared to $CuFe_2O_4$, is a potential source of soluble iron during leaching of copper calcines.[42] According to Blanks,[43] $CuFe_2O_4$ and $CuSO_4$ do not coexist but react to form $CuO \cdot CuSO_4$ and Fe_2O_3, *viz.*:

$$\underset{(c)}{CuFe_2O_4} + \underset{(c)}{CuSO_4} \rightarrow \underset{(c)}{CuO \cdot CuSO_4} + \underset{(c)}{Fe_2O_3} \qquad [21]$$

Floyd and Willis[42] have examined the system Cu-Fe-O and shown that $CuFeO_2$ exists over a wide range of oxygen partial pressures and that even high oxygen partial pressures do not ensure that $CuFeO_2$ will be absent in the calcine.

Thermodynamic data for $CuFe_2O_4$ and $CuFeO_2$ are not well established.[44–48] To examine the thermodynamic possibility of the formation of copper ferrites in the Cu-Fe-Ca-S-O system, data for $CuFeO_2$ were obtained from Eriksson and Rosen[44] and that for $CuFe_2O_4$ from Jacob *et al.*[46] Disregarding formation of calcium ferrites, thirty-eight possible equilibria pertaining to copper ferrites were examined, and possible bivariant equilibria in the Cu-Fe-Ca-S-O systems are shown in Figures 17(a) and 17(b).

Equilibria of interest together with their equilibrium constants are listed in Table XI. For the ferrites considered (Eqs. xix-xxii), equilibrium constants range typically from 1×10^{-3} to 1×10^{-9}. In this case, due to the partial pressure of SO_2 over the system, the thermodynamic conditions are unfavorable for the formation of ferrites. However, if SO_2 is removed from the system as soon as it forms, the equilibria would continuously be displaced to the right. Displacement may result from either: (a) employment of extremely high gas flow-rates, and/or (b) addition of CaO.

Eq. xxiii in Table XI shows the potential of CaO for removal of SO_2 from the system. Due to the large equilibrium constant, CaO removes SO_2 continuously and displaces the ferritization equilibria to the right at all temperatures. Thus, energetically, we may anticipate the formation of ferrites under all roasting conditions investigated for the L.C.P.R.-Process.

The thermodynamic analyses are supported by X-ray diffraction patterns from the periphery and core of the pellet roasted at 773 K and $G = 0.0015$ gm/cm^2 s. Examination of the patterns supports the suggestion that due to the presence of CaO insufficient SO_2 exists to cause significant sulfation of copper sulfides to $CuSO_4$ and that diminishing amounts of sulfate type phases, *i.e.*, $CuSO_4$, $CuO \cdot CuSO_4$, and $FeSO_4$, would be found. The major phases found were α-Fe_2O_3, $CaSO_4$, and CuO in both the core and periphery. Traces of phases forming under low oxygen potentials (Fe_3O_4, $FeSO_4$, CaS, and $Cu_{2-x}S$) were found in the sample core and were probably due to oxygen deficiency resulting from increased diffusional resistance in the product layer. Copper ferrites ($CuFeO_2$, $CuFe_2O_4$) were found in both the core and periphery.

That the major oxidation product in the calcines is CuO and is due to lime addition is also apparent from an examination of leaching results reported by Davis,[7] Table XII. Comparison of leaches (Nos. 28 and 29) from calcines with and without addition of lime show a marked reduction in copper extraction in deionized water. Had the oxidation product been $CuSO_4$, no reduction should have occurred. Bartlett and Haung[4] have reported that at 773 K most of

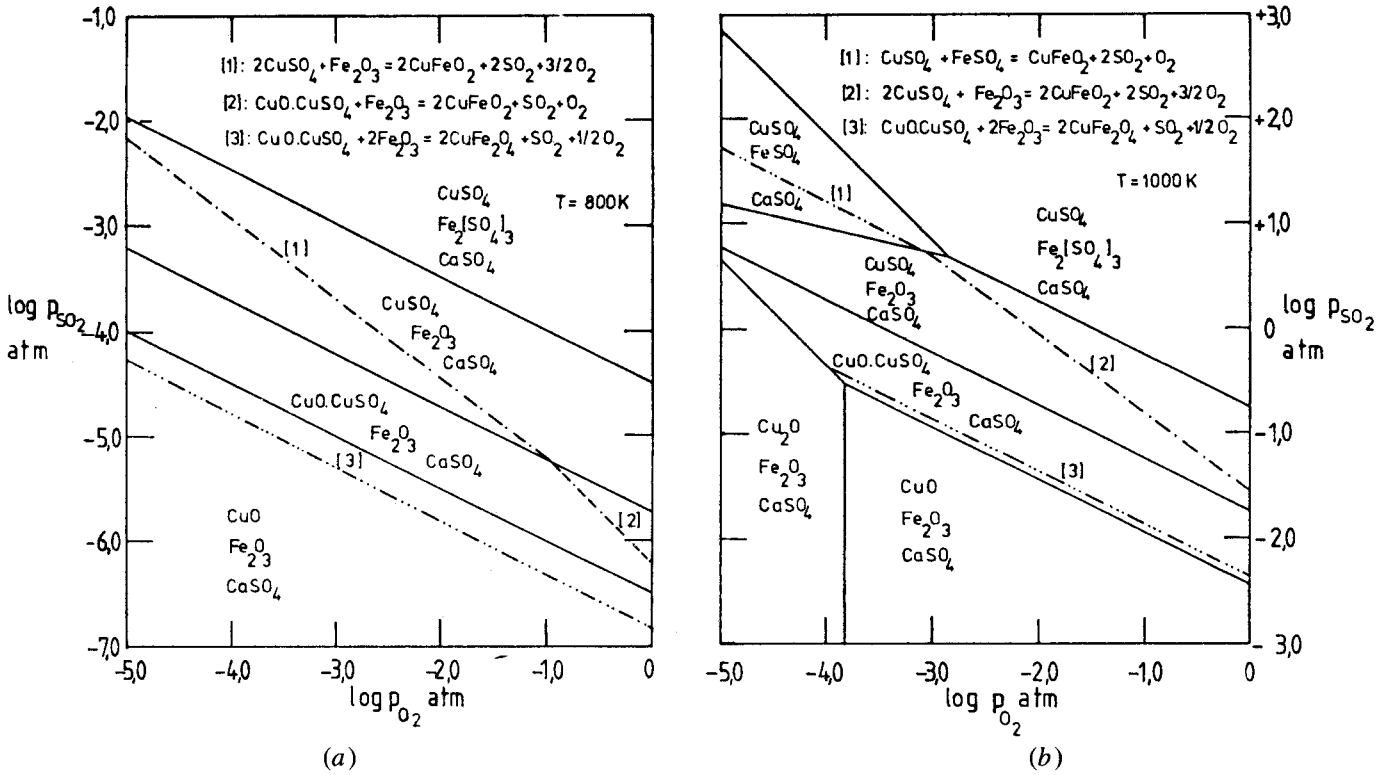

Fig. 17 — (*a*) Bivariant equilibria for formation of ferrites with respect to the Cu-Fe-S-O system in the Cu-Fe-Ca-S-O system at 800 K. (*b*) Bivariant equilibria for formation of ferrites with respect to the Cu-Fe-S-O system in the Cu-Fe-Ca-S-O system at 1000 K.

Table XI. Equations xix to xxii List Possible Bivariant Equilibria in the Cu-Fe-S-O System; Equation xxiii Incorporates the Sulfation Equilibria in the Ca-S-O System.

Number	Reaction	Equilibrium Const. K_{eq} 800 K	1000 K
xix	$2CuSO_4$ (c) + Fe_2O_3 (c) ⇆ $2CuFeO_2$ (c) + $2SO_2$ (g) + $\frac{3}{2}O_2$ (g)	1.3×10^{-12}	721.1×10^{-6}
xx	$CuSO_4$ (c) + $FeSO_4$ (c) ⇆ $CuFeO_2$ (c) + $2SO_2$ (g) + O_2 (g)	1.7×10^{-9}	25.0×10^{-3}
xxi	$CuO \cdot CuSO_4$ (c) + Fe_2O_3 (c) ⇆ $2CuFeO_2$ (c) + SO_2 (g) + O_2 (g)	613.8×10^{-9}	39.7×10^{-3}
xxii	$CuO \cdot CuSO_4$ (c) + $2Fe_2O_3$ (c) ⇆ $2CuFe_2O_4$ (c) + SO_2 (g) + $\frac{1}{2}O_2$ (g)	155.6×10^{-9}	4.2×10^{-3}
xxiii	CaO (c) + SO_2 (g) + $\frac{1}{2}O_2$ (g) ⇆ $CaSO_4$ (c)	818.5×10^{15}	231.2×10^{9}

Table XII. Results of Aqueous Leaching as Investigated by Davis[7]

Leach Number	Pellet Roast Temperature, K	Stoich. Lime Comp., Pct	Wt. Green Pellets gms.	Wt. of Cu in Pellets gms.	Wt. of Cu in Leach Liquor gms.	Copper Extraction Pct	Comments
28	793	0	0.9482	0.2579	0.1105	42.85	**
29	793	100	0.6806	0.1035	21.05E-6	0.02	**

**Pellets crushed and leached in deionized water at 323 K for 24 hours

the copper was converted to $CuSO_4$ which could be easily leached, and the bulk of the iron remained as acid-insoluble Fe_2O_3. This, however, was neither observed by Davis[7] nor in the present investigation and cannot be reconciled with the thermodynamics of the Cu-Fe-Ca-S-O system.

While there is no analysis available for iron reporting in the leach solution, a thermodynamic and X-ray diffraction appraisal indicates that an excessive quantity of iron may be anticipated in the leach solution. This observation is supported by the results reported by Haver and Wong,[5] Bartlett

and Prater,[8] and Pentz *et al.*:[11]

H_2SO_4 (gpl)	Fe (wt pct)	Cu (wt pct)	Ref.
30	39	80	5
60	13	95	11
80	10	95	8

Low copper extractions in the L.C.P.R.-Process also result from residual copper-iron-sulfide grains found in the calcines (Figures 13 and 18). Unreacted residual Cu-Fe-S may be a result of the crystal orientation of the grain[34] and/or due to insufficient exposure of the particle. Unreacted residue may also result from nonuniformity of the chemical reactivity of the sulfide. The more reactive chalcopyrite grain with a lower activation energy reacts to completion while a less active grain remains unreacted.[33] X-ray diffraction analyses of the calcine indicate that the grains contain both high temperature forms of copper sulfide (Cu_2S, 773 K) and diginite ($Cu_{1.96}S$, 773 K). This is in accordance with the observations of Thornhill and Pidgeon.[39]

B. *Efficiency of Sulfur Fixation in the L.C.P.R.-Process*

A maximum of 93 wt pct sulfur fixation was achieved, and variation in lime source only marginally influenced sulfur retention. Total sulfur fixations, however, were somewhat lower than those reported by other studies, Table I. Lower sulfur fixation may be due to the use of hypostoichiometric amounts of lime for the roast and/or a result of varying reactivities of lime types.[38,49,50] Figure 19 summarizes the results of a recent investigation of the L.C.P.R.-Process by Yusuf and Suranatha.[49] Low sulfur fixation was suggested to result from the exothermic nature of the system (100 to 200 K rise above the furnace temperature) and from the subsequent decomposition of $CaSO_4$. This observation defies the sulfation equilibria for $CaSO_4$ presented in Figure 1 which shows that $CaSO_4$ is stable over this temperature range. Lower sulfur fixation may instead be the result from either variable lime reactivity, densification of the sulfate product layer around individual CaO grain, or from the mode of pellet preparation. Below a "critical" size, the pellet may be too small to retain SO_2 within the pellet for sufficient period to react efficiently with the lime.

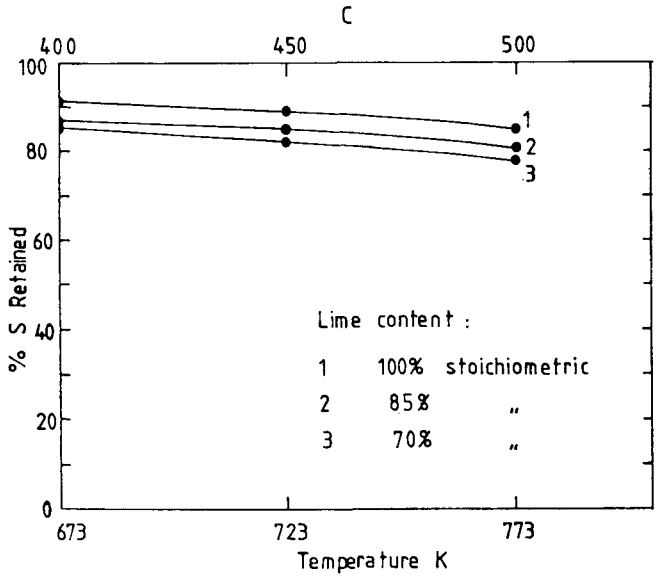

Fig. 19 — Variation of sulfur fixation with lime addition according to Yusuf and Suranatha.[49]

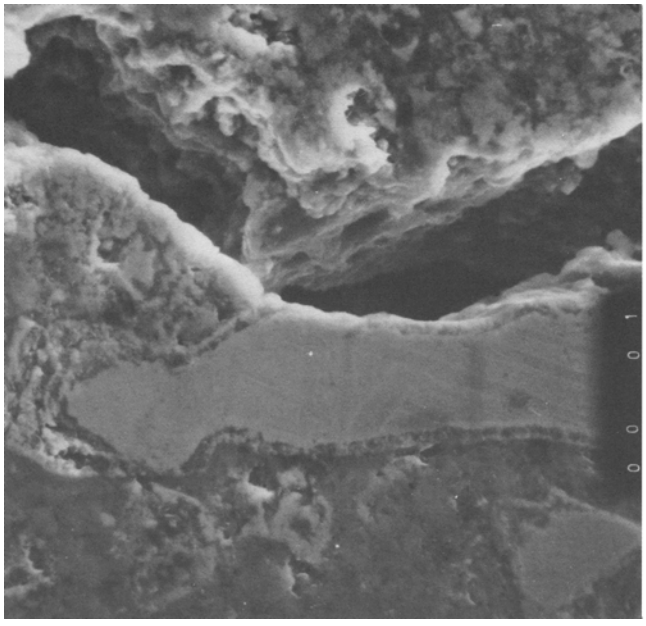

(*a*)

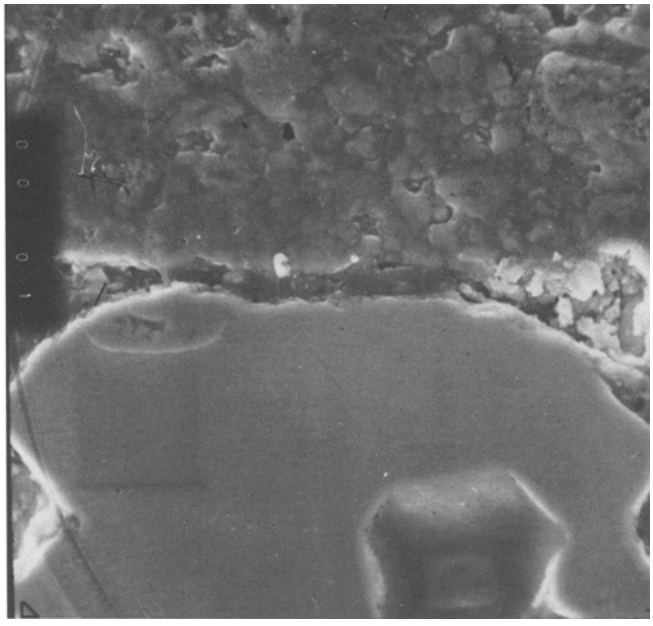

(*b*)

Fig. 18 — Unreacted copper-iron-sulfide particles in a completely reacted lime-concentrate pellet from a 773 K roast.

VI. CONCLUSIONS

The present results substantiate that in spite of a Re_p number of 4.1 (Sh = 3.1) and qualitative analyses suggesting insignificance of boundary layer influence, convective mass transfer cannot be ignored. Overall pellet oxidation appears to proceed by mixed control involving oxygen boundary layer diffusion and diffusion through the product layer.

Secondly, as the true oxidation stoichiometry for the lime-concentrate pellet roasting is only approached asymptotically with the advance of the interface into the pellet, *per se* measured rates are "apparent" reaction rates and give only an indication of the true oxidation reaction.

The reaction stoichiometry is sensitive to oxygen potential and is complicated by sintering. Pellet sintering occurs at 773 K and 873 K but is more pronounced at the higher temperature. Massive sintering at 873 K substantially retards the rate of oxidation. Roasting to completion is also crucially dependent on the mode of pelletization and pellet density.

Heat transfer to the reaction interface is without influence on the oxidation rate.

Failure of leaching to achieve appropriate extraction is attributable to the inherent function of the lime addition in promoting ferritization at all roast temperatures. The ferrites are uniformly distributed in the pellet and result not only in lowered copper recoveries but also in significant iron transfer into the leach solution.

Sulfur fixation by lime meets the 10 wt pct statutory regulation; however, sulfur arrest achieved by limes from various sources is a function of the reactivity of the lime type, and each individual lime has to be extensively investigated to ascertain its reactivity in the Lime-Concentrate-Pellet-Roast Process.

SYMBOLS

1, 2	specie notation
b, g, i, o, p, r	(Subscripts) bulk, gas, internal, outer, pellet, reaction conditions, respectively
c_p	specific heat at constant pressure
d	diameter
h, h_T	heat transfer coefficients
$h_{ov}, h_{rad}, h_{conv}$	heat transfer coefficients for overall, radiative, and convective conditions
k	thermal conductivity
m_0, m_t, m_f	initial mass, mass at time t, and final mass
$\dot{n}, \dot{n}_{in,ob}, \dot{n}_{in,th}$	rate of reaction, initial observed rate, and initial theoretical rate
$\dot{q}$	rate of heat flow
r	radius
$r^* = r_i/r_o$	fractional radius
t	time
u	superficial gas velocity
$\dot{v}$	volumetric flow rate
w	weight
D, D_{eff}	diffusivity, effective diffusivity
E	emissivity
$F = 1 - r^*$	fractional reaction
$G = \rho_g u_p$	mass velocity
ΔH_r	enthalpy change in reaction
K, K_{Eq}	equilibrium constant
M	molecular weight
P, P_{Eq}	pressure, pressure at equilibrium
R	gas constant, mechanical units
T	temperature
$Nu = hd/k$	Nusselt number
$Pr = \mu c_p/k$	Prandtl number
$Re = dG/\mu$	Reynolds number
$Sc = \mu/\rho D_{12}$	Schmidt number
$Sh = \alpha d/D_{12}$	Sherwood number
α	convective mass transfer coefficient
μ	viscosity
ρ	density
σ	Stefan-Boltzmann Constant, 5.6703E-08 W/m^2K^4
σ^*	Lennard-Jones Force Constant
ϕ_{MT}	fraction of initial reaction resistance due to mass transfer defined by Eq. 9.0
Δ	change in parameter
Ω_D	collision integral for diffusion

ACKNOWLEDGMENTS

The authors thank Professor H. Muir, School of Metallurgy, University of New South Wales, Australia, for the provision of facilities for this work, Gatt, and the Australian Government for provision of a fellowship to H.A.

REFERENCES

1. G. M. Swinkles and R. M. Berezawsky: *CIM Bull.*, 1978, vol. 71, pp. 105-21.
2. A. J. Parker, D. M. Muir, D. E. Giles, R. Alexander, J. O'Kane, and J. Avraamides: *Hydrometallurgy*, 1975, vol. 1, pp. 169-81.
3. Anon: *Engg. Min. J.*, 1977, vol. 178, p. 33.
4. R. W. Bartlett and H. H. Haung: *J. Met.*, 1973, vol. 25, no. 12, pp. 28-34.
5. F. P. Haver and M. M. Wong: Report Invest., R. I. 8006, U.S. Bureau of Mines, 1975.
6. I. White: Research Report, R.I. 780-1, Mt. Lyell Mining and Railway Co. Ltd., Tasmania 7467, Australia.
7. A. Davis: M. App. Sci. Thesis, University of New South Wales, Australia, 1975.
8. R. W. Bartlett and J. D. Prater: Kennecott Copper Corporation, Metal Mining Div. Research Center, Salt Lake City, UT, unpublished research, 1977.
9. A. Triandaf, V. Mavromati, and F. Olaru: *Inst. Cer. Chemice*, 1962, vol. 2, pp. 185-219. Abstract in ASM Rev. of Metall., Cit. 65-11 MO2-32294, 65-H.
10. F. P. Haver and M. M. Wong: *Min. Engg.*, 1972, vol. 24, pp. 52-53.
11. R. D. Pentz, P. R. Jochens, T. H. Tunley, J. L. Marran, and T. G. Murphy: Report No. 1772, National Institute of Metallurgy, Johannesburg, S.A., November 1975.
12. C. W. Dannat and H. J. T. Ellingham: *Disc. Farad. Soc.*, 1948, vol. 4, pp. 126-39.
13. V. N. G. Schmahl: *Archiv. Eisenhuttenwesen*, 1954, vol. 25, pp. 315-19.
14. H. H. Kellogg and S. K. Basu: *Trans. TMS-AIME*, 1960, vol. 218, pp. 70-81.
15. C. B. Alcock: *Can. Metall. Q.*, 1971, vol. 10, pp. 287-89.
16. T. Rosenqvist: *Principles of Extractive Metallurgy*, McGraw-Hill Book Co., New York, NY, 1974, pp. 245-55.
17. R. O. Thomas and D. W. Hopkins: *Trans. IMM Sect. C*, 1973, vol. 82, pp. C243-C245.
18. J. F. C. Fisher: *Trans. IMM*, 1963-1964, vol. 73, pp. 109-16.
19. H. H. Kellogg: *J. Metals*, 1956, vol. 8, pp. 1105-11.
20. M. B. Shirts, P. A. Bloom, and W. A. McKinney: Report Invest. R. I. 7996, U.S. Bureau of Mines, 1975.
21. Index (Inorganic) to the Powder Diff. File: ASTM Special Tech. Publ. 48-M2, 1963.

22. J. M. Skeaff and A. W. Espelund: *Can. Metall. Q.*, 1973, vol. 12, pp. 445-54.
23. J. Szekely and N. J. Themelis: *Rate Phenomena in Process Metallurgy*, J. Wiley and Sons Inc., New York, NY, 1971, pp. 601-38.
24. W. E. Ranz: *Chem. Eng. Prog.*, 1952, vol. 48, pp. 247-53.
25. *CRC Handbook of Chem. Phys.*: 57th ed., Chem. Rubber Co. Press Inc., Cleveland, OH, 1976, p. F-9.
26. T. R. Marrero and E. A. Mason: *J. Phys. Chem. Ref. Data*, 1972, vol. 1, pp. 3-118.
27. N. A. Warner: *Trans. TMS-AIME*, 1964, vol. 230, pp. 163-76.
28. M. Jakob and G. A. Hawkins: *Elements of Heat Transfer*, 3rd ed., J. Wiley and Sons Inc., New York, NY, 1957, p. 239.
29. A. V. Bradshaw: *Trans. IMM Section C*, 1970, vol. 79, pp. C281-C294.
30. A. W. D. Hills: *Chem. Eng. Sci.*, 1968, vol. 23, pp. 297-320.
31. A. W. D. Hills: *Metall. Trans. B*, 1978, vol. 9B, pp. 121-28.
32. H. H. Haung and R. W. Bartlett: *Metall. Trans. B*, 1976, vol. 7B, pp. 369-74.
33. L. S. Leung: *Metall. Trans. B*, 1975, vol. 6B, pp. 341-43.
34. A. P. Prosser: School of Metallurgy, Univ. of New South Wales, N.S.W. 2033, Australia, Commonwealth Min. Metall. Congress, 1969, unpublished report, 1969.
35. K. S. Murthi, D. Harrison, and R. K. Chan: *Environ. Sci. Tech.*, 1971, vol. 5, pp. 776-81.
36. J. Szekely and C. Karatas: *Metall. Trans. B*, 1978, vol. 9B, pp. 147-50.
37. A. B. Whitehead and R. W. Urie: *Proc. Australas. Inst. Min. Metall.*, 1961, vol. 119, pp. 51-85.
38. M. Hartman and R. W. Coughlin: *AIChE. J.*, 1976, vol. 22, pp. 490-98.
39. P. G. Thornhill and C. M. Pidgeon: *J. Metals*, 1957, vol. 9, pp. 989-95.
40. A. W. D. Hills: *Heat and Mass Transfer in Process Metallurgy*, Int. Min. Metall., London, 1967, pp. 39-77.
41. D. C. Lynch and J. F. Elliot: *Metall. Trans. B*, 1978, vol. 9B, pp. 691-704.
42. J. M. Floyd and G. M. Willis: *Australas. Inst. Min. Metall. Monograph 2*, Melbourne, 1961, pp. 61-64.
43. R. F. Blanks: Ph.D. Thesis, Univ. of Melbourne, 1961.
44. G. Eriksson and E. Rosen: *Scand. J. Metall.*, 1971, vol. 3, pp. 94-96.
45. K. T. Jacob, K. Fitzner, and C. B. Alcock: *Metall. Trans. B*, 1977, vol. 8B, pp. 451-60.
46. T. Rosenqvist: *Metall. Trans. B*, 1978, vol. 9B, pp. 337-51.
47. E. G. King, A. D. Mah, and L. B. Pankratz: *Thermodynamic Properties of Copper and its Inorganic Compounds*, INCRA Monograph II, International Copper Research Association Inc., New York, NY, 1973.
48. R. H. Borgwardt: *Environ. Sci. Technol.*, 1972, vol. 6, pp. 350-60.
49. Yusuf and W. Suranatha: Lembaga Metallurgi, Nasional-LIPI, Indonesia, Seminar Pentataran Pirometallurgi, Bandung, Indonesia, 19-22 February 1979, unpublished research, 1979.
50. T. R. Ingraham: *Trans. TMS-AIME*, 1965, vol. 233, pp. 359-63.
51. O. Kubaschewski, E. Evans, and C. B. Alcock: *Metallurgical Thermochemistry*, 4th ed., Pergamon Press, Oxford, 1967, p. 312.
52. M. Nagamori and F. Habashi: *Metall. Trans.*, 1974, vol. 5, pp. 523-24.
53. R. L. Benner and H. Kenworthy: Report Invest. R.I. 6769, U.S. Bureau of Mines, 1966.
54. JANAF Thermochemical Tables: 2nd ed. NSRDS-NBS 37, Nat. Bureau Stand., June 1971.
55. JANAF Thermochemical Tables; 1975 Supplement: *J. Phys. Chem. Ref. Data*, 1975, vol. 4, p. 1.
56. JANAF Thermochemical Tables; 1978 Supplement: *J. Phys. Chem. Ref. Data*, 1978, vol. 7, p. 793.